Nano Energy 117 (2023) 108857

Contents lists available at ScienceDirect

Nano Energy

journal homepage: www.elsevier.com/locate/nanoen

3D-printed conducting polymer hydrogel-based DC generator for self-powered electromechanical sensing

Ruizhe Yang [a,b,1], Zipeng Guo [c,d,e,1], Zhaohan Yu [f], Fengyin Du [g], Vashin Gautham Nanjangud Thyagaraja [a,b], Leqi Lin [a,b], Dylan R. Yu [h], Pengchong Xu [i], Jason N. Armstrong [a], Shaoting Lin [f], Chi Zhou [c,*], Jun Liu [a,b,**]

[a] Department of Mechanical and Aerospace Engineering, University at Buffalo, The State University of New York, Buffalo, NY 14260, USA
[b] RENEW (Research and Education in Energy, Environment and Water) Institute, University at Buffalo, The State University of New York, Buffalo, NY 14260, USA
[c] Department of Industrial and Systems Engineering, University at Buffalo, The State University of New York, Buffalo, NY 14260, USA
[d] Department of Industrial and Systems Engineering, Rochester Institute of Technology, Rochester, NY 14623, USA
[e] AMPrint Center, Rochester Institute of Technology, Rochester, NY 14623, USA
[f] Department of Mechanical Engineering, Michigan State University, East Lansing, MI 48824, USA
[g] Jiangsu Key Laboratory of Construction Materials, School of Materials Science and Engineering, Southeast University, Nanjing 211189, PR China
[h] Pittsford Mendon High School, Pittsford, NY 14534, USA
[i] Department of Electrical and Computer Engineering, Rutgers, The State University of New Jersey, Piscataway, NJ 08854, USA

ARTICLE INFO

Keywords:
Self-powered devices
Electromechanical sensing
Additive manufacturing
Ionic-electronic conduction
Conductive hydrogel
Flexible electronics

ABSTRACT

Self-powered electromechanical sensing has gained considerable attention for its potential to transform diverse applications, such as wearable electronics, robotics, artificial intelligence, and environmental monitoring. One promising technology emerging in this field is additive manufacturing of conductive hydrogels as elementary component for energy harvesting/storage, enabling robust, flexible, and biocompatible sensor devices. In this study, we demonstrate a continuous 3D printed conductive hydrogel-based energy harvesting device with triply periodic minimal surface (TPMS) architecture. Leveraging the feature of direct-current (DC) energy generation upon mechanical stimulation, the device is capable of self-powered sensing operations. The DC energy generation mechanisms are discussed with the consideration of multiple physiochemical factors. Notably, the printed 3D architected conductive hydrogel (3D-ACH) exhibits robust mechanical properties, providing high flexibility with over 50% compressive strain. Additionally, we explore its performance as a pressure/strain sensor to achieve self-powered sensing capabilities. The combination of 3D-printed conductive hydrogels and energy generation capabilities represents a promising approach towards achieving self-powered sensing capabilities.

1. Introduction

Self-powered wearable and implantable applications have emerged as a promising field in recent years, offering innovative solutions for powering electronic devices without the need for external energy sources [1,2]. The concept of self-powered wearables and implants allows for the efficient conversion of ambient energy, such as body heat, motion, or light, into electrical energy to power the associated electronics [3–5]. By eliminating the need for traditional power sources, self-powered devices offer enhanced convenience, prolonged usage, and increased mobility for users [6,7]. Additionally, the integration of electromechanical sensing capabilities enhances the functionality of these systems, enabling the detection and measurement of various physical parameters [8,9]. These devices have the ability to monitor vital signs, track physical activities, measure environmental parameters, and even enable advanced functionalities like gesture recognition or voice control [10,11]. Through the seamless integration of power generation and sensing capabilities, self-powered devices are poised to revolutionize personal healthcare, enhance user experiences, and redefine the boundaries of human-machine interaction [12]. Ongoing research and development

* Corresponding author.
** Corresponding author at: Department of Mechanical and Aerospace Engineering, University at Buffalo, The State University of New York, Buffalo, NY 14260, USA.
E-mail addresses: chizhou@buffalo.edu (C. Zhou), jliu238@bufflao.edu (J. Liu).
[1] These authors contributed equally

https://doi.org/10.1016/j.nanoen.2023.108857
Received 10 July 2023; Received in revised form 11 August 2023; Accepted 31 August 2023
Available online 3 September 2023
2211-2855/© 2023 Elsevier Ltd. All rights reserved.

efforts primarily focus on mechanisms such as piezoresistance [13,14], capacitance [15,16], and the triboelectric/tribovoltaic effect [17–19] for sensing electronic devices in wearable and implantable form factors. Although concentrated efforts have been devoted in electromechanical sensing field, each approach still has its own advantages and limitations. Piezoresistive sensors, for example, offer benefits such as high sensitivity, simple fabrication, and compatibility with existing semiconductor processes [20]. However, they may be susceptible to issues such as hysteresis, temperature dependence, and limited dynamic range. Sensing based on capacitive effect, on the other hand, provide advantages such as high sensitivity, low power consumption, and non-intrusiveness [21]. Nevertheless, they suffer from environmental factors like humidity and require careful calibration. Tribovoltaic or triboelectric sensing devices offer advantages such as self-powering capability, simplicity, and potential miniaturization [22]. However, they may encounter challenges in achieving high sensitivity and stability. Moreover, conventional triboelectric sensors often struggle with low current density generation and reliance on alternating current (AC) power.

Recently, to address the prevailing challenges, a novel solution has surfaced in the form of integrating conducting polymers with hydrogels [23]. Conducting polymers, such as poly(3,4-ethylenedioxythiophene): poly(styrenesulfonate) (PEDOT:PSS), have gained significant attention in various applications such as organic light-emitting diodes [24], energy harvesting [11,25], energy storage devices [26], biosensor/bioelectrodes [27], and wearable electronics [28] due to their exceptional properties, such as high electrical conductivity, flexibility, and biocompatibility. On the other hand, hydrogels possess remarkable characteristics, including high transparency, flexibility, stretchability, self-adhesion, excellent biocompatibility, and structural similarity to natural soft tissues [29]. These advantageous properties make hydrogels promising substrates for developing flexible strain sensors, particularly in the field of stretchable, transparent, and wearable pressure/strain sensors [30]. Consequently, the integration of conducting polymers and hydrogels offers the potential for direct utilization as sensing materials in wearable and implantable applications, owing to their excellent electrical performance, biocompatibility, and stretchability [31,32]. Exploiting the unique advantages of combining high electronic and mechanical performance, recent studies have reported the development of soft conductive hydrogel-based flexible sensors capable of converting external stimuli into electrical signals [33,34]. Moreover, the emergence of additive manufacturing techniques, such as 3D printing, has provided a powerful tool for working with hydrogels [35,36]. This integration enables rapid and customizable fabrication of intricate geometries, facilitating the production of complex structures with integrated functionalities [37,38]. However, current research endeavors are mainly focus on inkjet printing and fused deposition modeling, resulting in either simple layers or rough bulky bricks. Consequently, the complexity and quality of the printed objects are severely constrained, thus imposing limitations on its functionalities.

Vat photopolymerization process is a light projection-based 3D printing technique that utilizes photocurable liquid material, such as hydrogel, to fabricate 3D models. By incorporating a gas-permeable PDMS (Polydimethylsiloxane) vat substrate, a gas-inhibition zone is formed, allowing for the continuous printing of low-viscosity hydrogel materials [39]. The continuous vat photopolymerization approach shortens the fabrication time from hours to minutes, preventing hydrogel degradation in the conventional layer-by-layer printing process, thus ensuring the high-shape fidelity of the 3D-printed samples. On top of a fast 3D fabrication process, the development of conductive hydrogels necessitates softness and high durability [30,40]. However, hydrogel networks inherently suffer from brittleness, which poses a challenge for long-term usage in sensing applications [41]. To mitigate this challenge, the TPMS structures are designed for the 3D-printed conductive hydrogels. The TPMS structures feature zero-mean curvature, minimizing stress concentration when subjected to external loads. By 3D printing conductive hydrogels in TPMS structures, it exhibits enhanced mechanical durability and large recoverable strain. With an increased surface area of the TPMS structures, it also enhances the efficiency of energy harvesting, facilitating reliable and long-lasting use in self-powered sensing applications.

In this study, we design a bottom-up additive manufacturing approach by which conductive hydrogel can be printed to 3D complex architectures (as shown in Fig. 1a) with high electrical conductivity while serving as a building block of electric generators used in self-powered electromechanical sensing applications. The employment of stereolithography printing enables ultrafine printing resolution even for highly curved structures, which further enhances the flexibility of the as-printed 3D-ACH. The approach employed in this study incorporates essential characteristics necessary for wearable and implantable electronics, including self-powering capability, flexibility/stretchability, mechanical robustness, bio-compatibility, and more (Fig. 1a). These integrated features would broaden the applications of hydrogel-based materials that feature self-powered capabilities and intricate structure such as structural sensing, wearable/implantable electronics and multifunctional medical support.

2. Materials and methods

2.1. Printable ink preparation

To prepare the printable ink, poly(3,4-ethylenedioxythiophene) polystyrene sulfonate (PEDOT:PSS) solution was first made by dissolving pellets of PEDOT:PSS (Sigma-Aldrich, dry re-dispersible pellets, sheet resistance $< 200\ \Omega$/sq) in deionized (DI) water at varying concentrations (0.1 wt%, 0.5 wt%, 1 wt%, 1.5 wt%, and 2 wt%), which was then supplemented with 5 wt% of ethylene glycol (EG, anhydrous, 99.8%, Sigma-Aldrich) to enhance the electrical conductivity. DI water was produced by a Barnstead™ Smart2Pure™ Water Purification System from Thermo Fisher Scientific and the resistivity of the DI water used here was measured to be 18.2 MΩ·cm. Next, Polyethylene glycol diacrylate (PEGDA, Mn=700, Sigma-Aldrich) was added to the solution at a weight ratio of 1:7 and subjected to ultrasonic mixing for an hour. To initiate photopolymerization, Lithium phenyl-2,4,6-trimethylbenzoylphosphinate (LAP, purity $\geq$ 95%, Sigma-Aldrich) was added to the mixture at 0.5 wt%. Finally, a light absorber, Quinoline yellow ($C_{18}H_{11}NO_2$, purity$\geq$ 95%, Sigma-Aldrich), was added at 0.05 wt %. All chemicals were used as purchased without further processing.

2.2. Stereolithography printing process

A custom-built mask image-based stereolithography printer was used to 3D print the conductive hydrogels. A DLP (Digital Light Processing) projector with ultraviolet (UV) wavelength illumination (385 nm) was used as the light source. The diamond lattice 3D model was sliced into 2D mask images using a custom-programmed slicing software with a layer thickness of 50 μm. The diamond type lattice structures, as shown in Fig. 1b, were modeled by using nTopology software (nTopology Inc., US). A cuboid geometry with dimensions of 15 mm by 15 mm by 15 mm was filled with diamond-type unit cell to create the 3D lattice structure.

2.3. Electromechanical DC power characterization apparatus

The electromechanical DC power characterization was conducted using a F105-IM IntelliMESUR® advanced motorized mechanical test frame manufactured by Mark-10, along with a FS05–05 force sensor. A metal probe/plate as the top moving electrode was securely attached to the force sensor, while the sample under investigation was affixed to a platform connected to a steel plate functioning as the bottom electrode. Data acquisition during the experiments was accomplished utilizing a Keithley DM6500 Digital Multimeter.

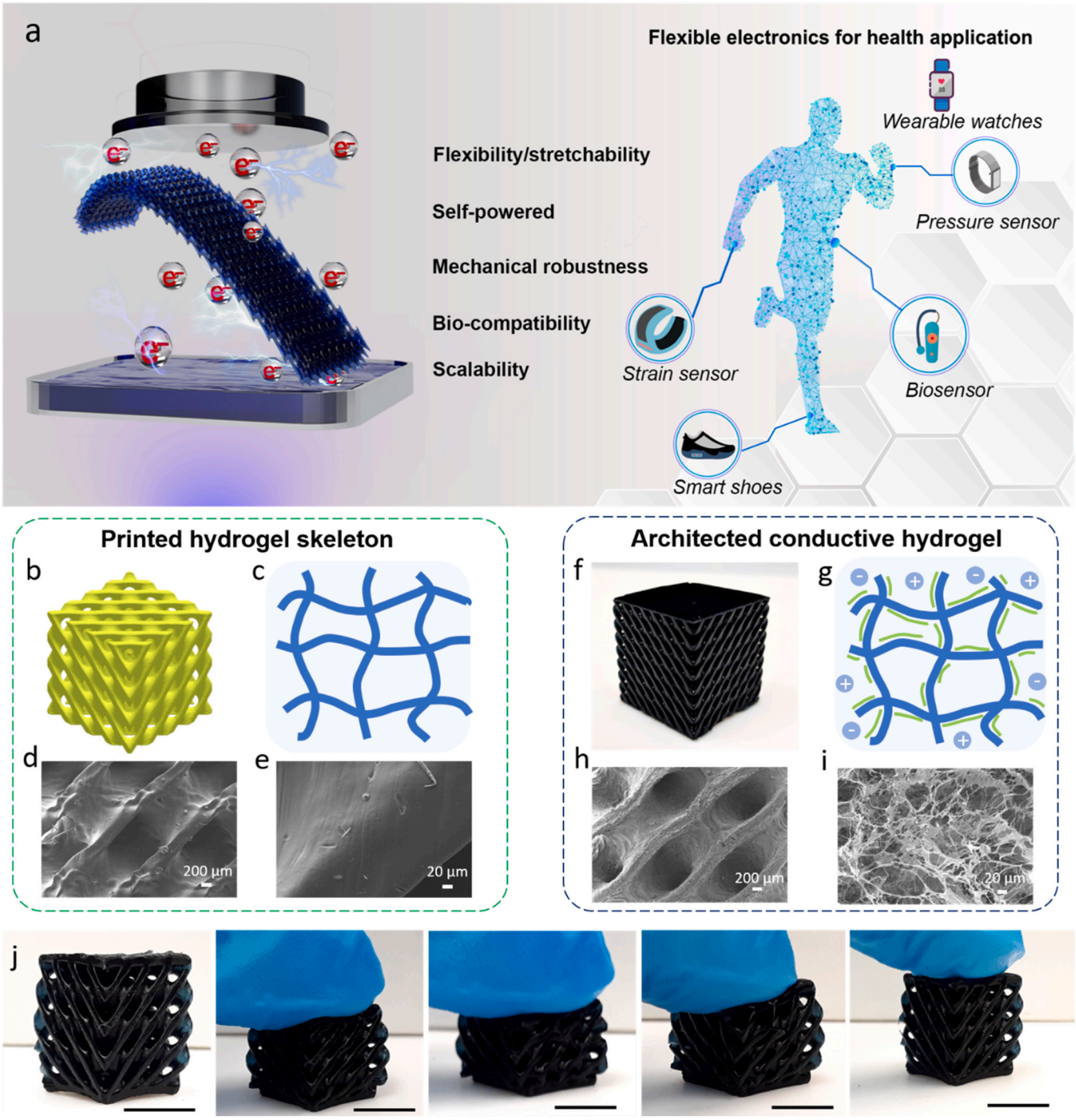


Fig. 1. (a) Schematic figure of 3D printing process and its potential wearable electronic applications; (b) lattice model, (c) schematic polymer chain structure and (d, e) SEM images of the printed hydrogel skeleton samples without PEDOT:PSS; (f) lattice model, (g) schematic polymer chain structure and (h, i) SEM images of the printed architected conductive hydrogel samples with PEDOT:PSS (j) The compressive recoverable printed architected conductive hydrogel lattice with 1.5 wt% PEDOT:PSS concentration. Scale bar is 10 mm.

2.4. Mechanical testing and finite element analysis (FEA)

The measurements of mechanical properties were performed utilizing an F105-IM IntelliMESUR® advanced motorized mechanical test frame from Mark-10 with FS05–10 and FS05–05 force sensors.

The mechanical behavior, especially the distribution of strain and stress in both bulk and structured hydrogels, was investigated by FEA implemented in ABAQUS (ABAQUS 2022, ABAQUS Inc.). To simulate the compression and release process, a cube bulk and a diamond structure were selected. The diamond structure was generated using the CAE tools developed by Flatt Pack [42]. For the analysis, the Ogden and Mullins effects model was employed to capture the nonlinear large deformation and molecular damage. The values of parameters μ, α, r and m were set as 110.725 kPa, − 3.186, 3.0 and 4.5 kJ m^{-3}, respectively.

3. Results and discussion

3.1. Fast stereolithography printing

The printable ink used in the vat photopolymerization process

contains PEGDA (Polyethylene glycol diacrylate), a photocurable component that undergoes crosslinking when exposed to UV light. This light-induced polymerization process is initiated by phonons, which carry energy to originate free-radical chain polymerization to solidify the hydrogel ink. Shown in Fig. 1d-e are the SEM images of the PEGDA network, revealing the porous polymer network. When adding PEDOT:PSS to the ink, it can be assembled within the PEGDA network to form the 3D TPMS structures as shown in Fig. 1h-i. PEDOT:PSS occupies the void space of the PEGDA network and carries positive and negative charges attached to the polymer network (Fig. 1g). As demonstrated in Fig. 1j, a finger compression/release of the as-printed conductive hydrogel with the TPMS structure (the Schwarz primitive model) exhibits zero mean curvature and seamless transitions between smooth minimal surfaces. This highlights the remarkable flexibility of the conducting hydrogel in its as-printed form when subjected to finger compression and release.

3.2. Energy harvesting characterization

The compression flexibility of the system is a result of the synergistic effect between a highly continuous curved architecture and a cross-linked polymeric network. This excellent flexibility enables enhanced tribovoltaic DC generation. Fig. 2a inset figure schematically demonstrates the DC power generation measurements, where an aluminum (Al) plate is used to tap the top surface of the printed conducting hydrogel with the assistance of a mechanical testing frame. As will be shown later, the purpose of using Al is to form Schottky contact with the conducting polymer hydrogel, which is one of the main features of dynamic DC generator [11]. The printed conductive hydrogel is positioned on an iron (Fe) thin film substrate (thickness, $d \approx 1$ mm), serving as the bottom electrode to complete the circuit. To verify the interfacial contact characteristics between Al top electrode and the printed conductive hydrogel, force-dependent current-voltage (I-V) characterization was performed on the Al/3D-ACH system. The obtained results, illustrated in Fig. 2b, exhibit a non-linear Schottky/ionic diode-like feature and demonstrate a positive correlation with respect to the applied force [43]. Moreover, the resistance of the Al/3D-ACH system was examined employing a two-wire configuration, as illustrated in Fig. 2c. As the concentration of PEDOT:PSS in the system increased from 0.1 to 2 wt%, a noticeable decrease in resistance was observed, with the resistance dropping dramatically from around 240 kΩ to 280 Ω. Furthermore, Fig. S3a illustrates the force value evolution during a typical 5-cycles tapping measurement with a presetting of 1.0 N. The corresponding open-circuit voltage (V_{OC}), short-circuit current (I_{SC}) and the

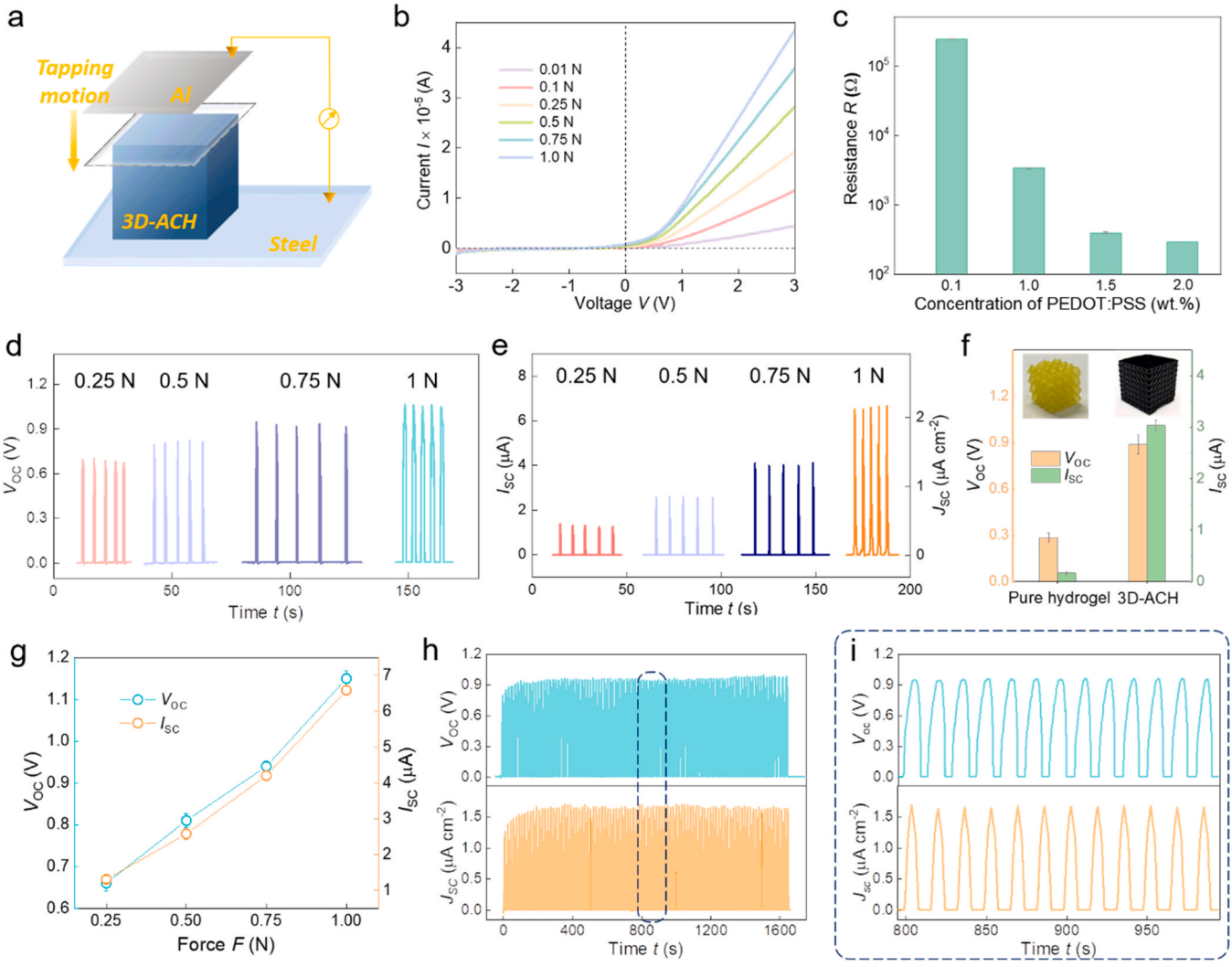


Fig. 2. (a) schematic figure of the power generation measurements; (b) Force-dependent I-V characterization of Al/3D-ACH system; (c) PEDOT:PSS concentration-dependent static two-wire resistance of Al/3D-ACH system; The (d) V_{OC} outputs and (e) and I_{SC} & J_{SC} outputs of typical 5-cycle tapping measurements under 0.25, 0.5, 0.75 and 1.0 N; (f) V_{OC} and I_{SC} outputs; (g) Tapping force-dependent V_{OC} and I_{SC} outputs. Inset: schematic figure of the power generation measurements; The continuous (h) V_{OC} and J_{SC} outputs and (i) Zoom-in detail of the Al and printed conducting hydrogel for over 200 cycles under tapping motion (tapping force: 1.0 N);.

corresponding current density (J_{SC}) are shown in Figs. 2d and 2e, respectively, with a V_{OC} of increased from 0.66 to 1.06 V and an I_{SC} boosted from 1.61 to 6.51 μA as the tapping force raised from 0.25 to 1.0 N. (testing sample: cubic length, l≈16 mm; contact area, A ≈ 256 mm^2). The modest rise in V_{OC} can be attributed to its generation mechanism (Fig. 2 g), which is commonly associated with the relative surface potential (work function) difference between the two contact materials involved, which in this case are Al and PEDOT:PSS. On the other hand, the generation of I_{SC} is influenced by multiple factors, including internal resistance (R), contacting area (A), etc, which implies those factors could be effectively employed as tuning parameters to enhance the compatibility of the conducting hydrogel (will discuss more in the later section). Therefore, the current enhancement is driven by the expansion of the microscopic contact area when subjected to external pressure.

To further examine the role of PEDOT:PSS in the power generation process, pure hydrogel samples have been prepared and examined under identical cyclic tapping experiments to assess their performance. The results, depicted in Fig. S4a-b, indicate that the V_{OC} and I_{SC} outputs are measured to be 0.28 V and 0.17 μA, respectively, during a standard 20-cycle tapping measurement (1.0 N). Comparative analysis between the V_{OC} and I_{SC} outputs of the pure hydrogel and 3D-ACH under identical experimental configurations (Fig. 2f) reveals that the pure hydrogel contributed to approximately 31% and 5% of the corresponding values, respectively. The observed voltage generation in the pure hydrogel can be attributed to the electrochemical interaction between the metal electrode and the structural water confined within the hydrogel matrix. On the other hand, the comparatively lower I_{SC} in the pure hydrogel sample is primarily ascribed to its significantly higher electrical resistance when compared to 3D-ACH. It is worth noting that the augmented I_{SC} performance of 3D-ACH is not solely ascribed to the intrinsic low electrical resistance of the conductive hydrogel but also facilitated by the enhanced charge mobility resulting from the electron hopping effect between the metallic domains of PEDOT:PSS. Moreover, Fig. 2h-i shows the V_{OC} and J_{SC} output under long-term cyclic testing (tapping force: 1.0 N; contact area: 100 mm^2), where both V_{OC} and J_{SC} output remains consistent over hundreds of cycles. This observation not only validates the durability and reliability of the printed conducting hydrogel for prolonged use but also indicates that the material retains its electrical properties and current generation capabilities even after extended periods of operation.

To gain insight into the underlying mechanism, we posit that the generation of DC power involves a combination of various driving forces, including 1) interfacial mechano-electronic excitation, 2) electrochemistry, and 3) ionic-electronic conduction (Fig. 3a). With regards to mechano-electronic excitation, our proposition suggests that the exertion of frictional energy at tapping interfaces induces the formation of energetic carriers, commonly referred to as the "tribovoltaic" effect [44]. Furthermore, as shown and discussed in Fig. 2,f, the electrochemistry effect also plays a significant role in DC power generation by facilitating the transfer of electrons between structural water, metal electrodes and PEDOT:PSS. This electron transfer occurs either at the interfaces or within the active materials of electrochemical systems. For example, in batteries and fuel cells, electrochemical reactions convert chemical energy into electrical energy. The flow of electrons between the anode and cathode, through redox reactions, generates a potential difference and subsequently a direct current. It is worth to point out that, as per our prior study, the electrochemical contribution to DC energy generation is heavily determined by the water content of the sample [12]. In our study, our attention was directed towards samples with low water content. These specimens were naturally dried and only contained water amount equivalent to the atmospheric moisture level. This choice

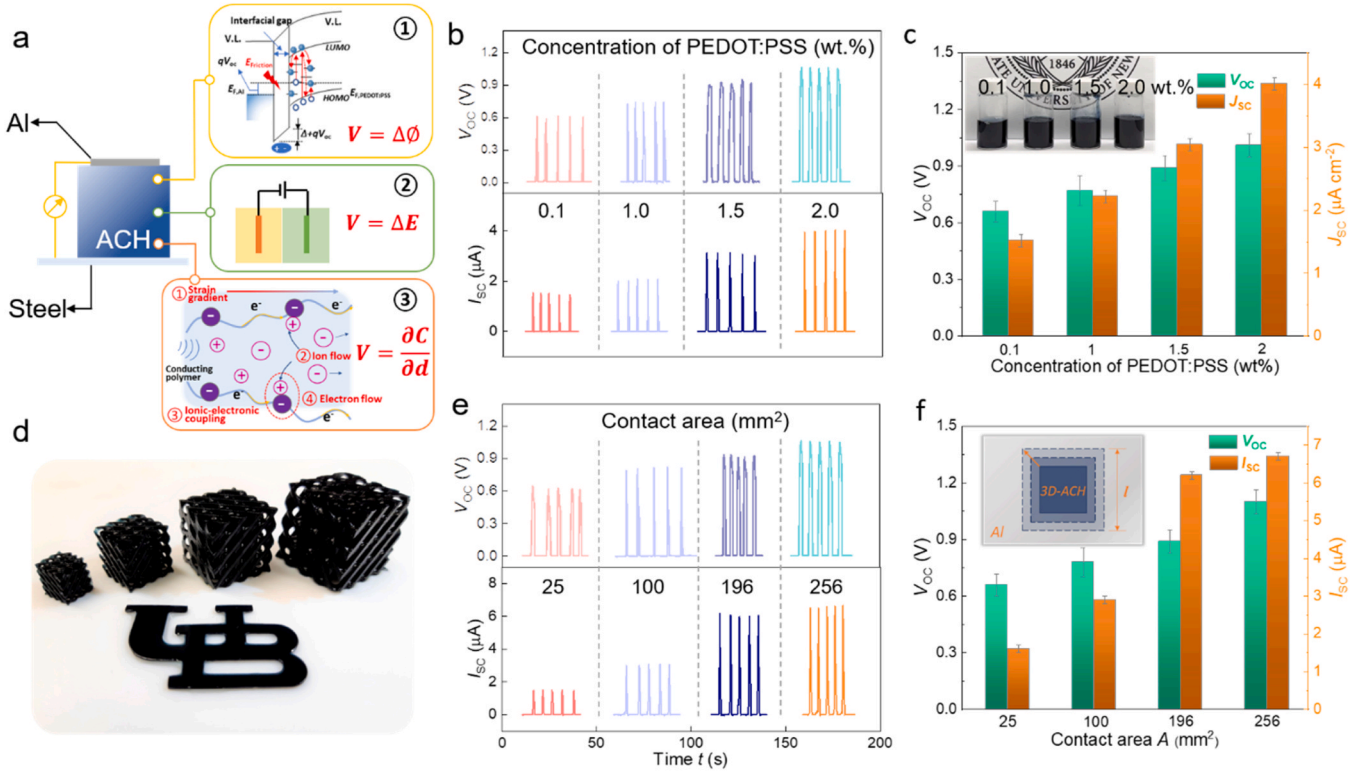


Fig. 3. (a) Schematic illustration of proposed DC power generation mechanism of 3D-ACH, 1) dynamic Schottky DC generation; 2) electrochemical effect; 3) ionic-electronic conduction; (b) PEDOT:PSS concentration-dependent V_{OC} and I_{SC} outputs (0.1, 1.0, 1.5 and 2.0 wt%); (c) PEDOT:PSS concentration-dependent V_{OC} and I_{SC} outputs under tapping motion (tapping force: 1.0 N), inset picture shows the precursor with different PEDOT:PSS concentrations: 0.1, 1.0, 1.5 and 2.0 wt%; (d) Optical photo of 3D-ACH samples with various cubic length; (e) Contact area-dependent V_{OC} and I_{SC} outputs (25, 100, 196 and 256 mm^2); (f) Contact area-dependent V_{OC} and I_{SC} outputs (tapping force: 1.0 N)), inset schematic picture demonstrates the contact area difference.

was driven by their remarkable mechanical properties and strong compatibility. Therefore, the electrochemical contribution should primarily arise from the presence of structural water encapsulated within the 3D-ACH sample. Last but not least, ionic-electronic conduction is a crucial phenomenon contributing to the generation of DC power. It involves the movement of both ions and electrons within a material or an electrolyte. In systems such as solid-state batteries or certain types of solar cells, ionic species like lithium ions migrate through solid-state electrolytes or across interfaces, while electronic carriers such as electrons or holes transport through the material to establish an electric current. In this case, it is proposed that the localized non-equilibrium ion gradient distribution under external stimuli induces ionic-electronic conduction, further contributing to the overall DC power generation of 3D-ACH. By considering these multiple driving forces, we can obtain a holistic understanding of the intricate processes underpinning DC power generation.

To better understand the influence of R and A on 3D-ACH samples, different printable precursors with varying concentrations of PEDOT:PSS have been prepared and utilized for printing the conducting hydrogel samples. This approach is taken because the conducting polymer, PEDOT:PSS, plays a dominant role in determining the conductivity of the printed conducting hydrogel. As shown in Fig. 3b-c, by adjusting the concentration of PEDOT:PSS in the printable precursors, the I_{SC} improved from 1.52 μA to 4.11 μA as the PEDOT:PSS concentration increased from 0.1 to 2.0 wt%, while the V_{OC} increased from 0.61 to 1.10 V (tapping force: ~ 1.0 N). Moreover, contact area-dependent DC generation measurement has also been designed and conducted by printing different conducting hydrogel with varying cubic sizes (Fig. 3d). As depicted in Fig. 3e-f, the I_{SC} demonstrates a notable increase, jumping from 1.51 to 6.61 μA as the contact area increases from 25 to 256 mm^2, when subjected to a tapping force of approximately 1.0 N. On the other hand, the V_{OC} experiences a rise from 0.63 to 1.15 V under the same testing parameters. These findings indicate that a higher concentration of PEDOT:PSS and a larger contact area contribute to improved conductivity, thereby enhancing the current generation capabilities of the printed conducting hydrogel. These approaches offer the flexibility to tailor the material's electrical properties and device configurations to meet specific requirements.

3.3. Mechanical behaviors of the printed hydrogel under cyclic compressive loads

To demonstrate the mechanical robustness of as-printed conductive hydrogel, cyclic compressive tests on bulk hydrogels and 3D-ACH samples were performed to examine their stress-strain behaviors and energy dissipation mechanisms under varying loads. The bulk hydrogel demonstrated a typical hyperelastic response as depicted in Fig. 4a. In contrast, the structured hydrogel exhibited a unique two-stage stress-strain behavior as shown in Fig. 4b, likely due to its diamond lattice architecture, which resulted in a bending-dominant behavior that led to a relatively flat stress-strain curve at small deformations and a significant stiffening at large deformation. To further characterize the mechanical dissipation at different strain levels, we calculate the hysteresis ratio h, which is defined as $h = \oint_0^{\varepsilon_{max}} S d\varepsilon / \int_0^{\varepsilon_{max}} S d\varepsilon$ with S being the nominal stress and ε being the corresponding strain. As shown in Fig. 4d, the structured hydrogel shows a larger mechanical dissipation compared with the bulk hydrogel, which suggests the crucial role of lattice architecture in promoting mechanical dissipation. We further assess the long-term durability of the 3D-printed structured hydrogel through cyclic compressive tests. As shown in Fig. 4e-f, the sample maintained consistent stress-loading distance curves and hysteresis ratios even after undergoing over 100 cycles of compressive loading. These findings suggest that the structured hydrogel is capable of enduring repeated mechanical loading for sustained energy harvesting performance.

To better understand the nonlinear large deformation, we utilized the Ogden-Mullins model in Abaqus to predict the stress-strain curve of the bulk and structured hydrogels respectively. The free energy function considering Mullins effect can be derived as [45].

$$W(\mathbf{F}, \eta) = \eta \widetilde{W}(\mathbf{F}) + \phi(\eta) \tag{1}$$

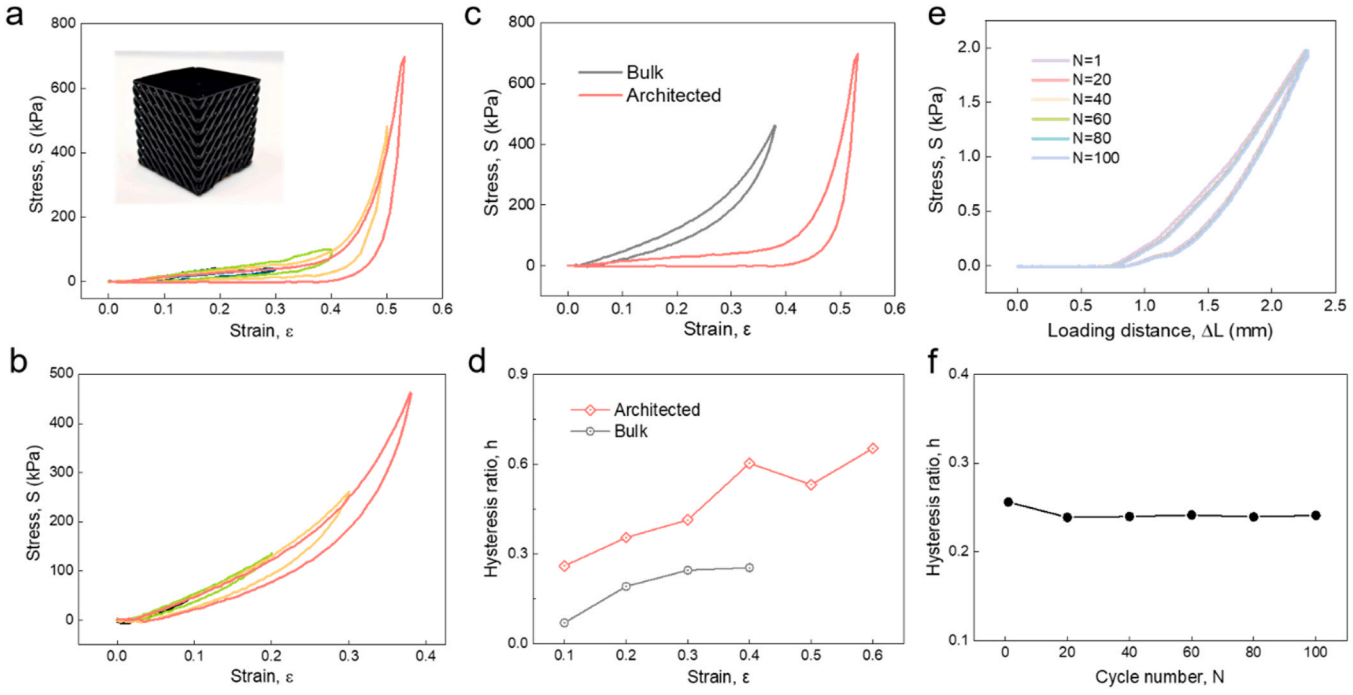


Fig. 4. Mechanical behaviors of bulk and structured hydrogels under cyclic compressive loads**; (a) Cyclic stress-strain curves of a structured hydrogel** at various strains; (b) **Cyclic stress-strain curves of a bulk** hydrogel at various strains; (c) Comparison of experimental and theoretical stress-strain curves between bulk and structured hydrogels; (d) Comparison of hysteresis ratios at various strains between bulk and structured hydrogels; (e) Long-term robustness analysis of a structured hydrogel (3D printed hydrogel lattice). N represents cycle number; (e) Stress-loading distance curves and (f) hysteresis ratios over 100 cycles of compressive loading.

where **F** denotes the deformation gradient tensor, the damage variable η indicates the extent of material damage and $\phi(\eta)$ is the damage function. $\widetilde{W}(\mathbf{F})$ represents the free energy function of a purely elastic material without the Mullins effect, which can be expressed by the first-order Ogden model and written as [46].

$$\widetilde{W} = \frac{2\mu}{\alpha^2}\left(\lambda^{\alpha} + 2\lambda^{-\frac{\alpha}{2}} - 3\right) \tag{2}$$

where μ and α are fitting parameters, and stretch λ can be calculated by $\lambda = 1 - \varepsilon$, where ε represents the compressive strain. By fitting Eq. (2) to the measured stress-strain curve of the bulk hydrogel, μ and α are identified as 110.725 kPa and − 3.186, respectively (Fig. 3a).

In addition, mechanical dissipation is an undeniable phenomenon in this process manifested by the hysteresis loop in the stress-strain curve. The toughening due to the presence of the hysteretic mechanical dissipation can be phenomenologically characterized using the Mullins effect, and the damage function $\phi(\eta)$ and damage variable η can be derived as [47].

$$\phi(\eta) = \int_1^{\eta} \left[(m + \beta W^m)\mathrm{erf}^{-1}(r(1-\eta) - W^m)\right] d\eta \tag{3}$$

$$\eta = 1 - \mathrm{erf}\left[(W^m - \widetilde{W}) \Big/ (m + \beta W^m)\right] \tag{4}$$

where W^m represents the maximum strain energy density of the material before unloading, and erf denotes the error function. β is a positive number used to prevent an overly stiff response during unloading from relatively large stretch levels. Besides, the parameters r and m denote the damage properties of the material, representing the maximum extent of material damage and the critical energy scale required for significant dissipation.

In our analysis, we employed the modified Ogden-Mullins model in Abaqus to determine the values of r and m as 3.0 and 4.5 kJ m^{-3}, respectively. The parameter of β is set as 0.1 for numerical stabilization. The fitted results agree well with the experimental data, as demonstrated in Fig. 5a and 5b. For the stimulation of structured hydrogel (Fig. 5c), we generated the diamond structure following the CAE tools developed by Flatt Pack [42]. Fig. 5d and Supplementary Video-1 display the stress fields of the structured hydrogel under compressive loading. Results indicate that there is indeed a region of significant dissipation at the central bulge due to stress concentration. The corresponding stress-strain curve and hysteresis ratio upon various strains are

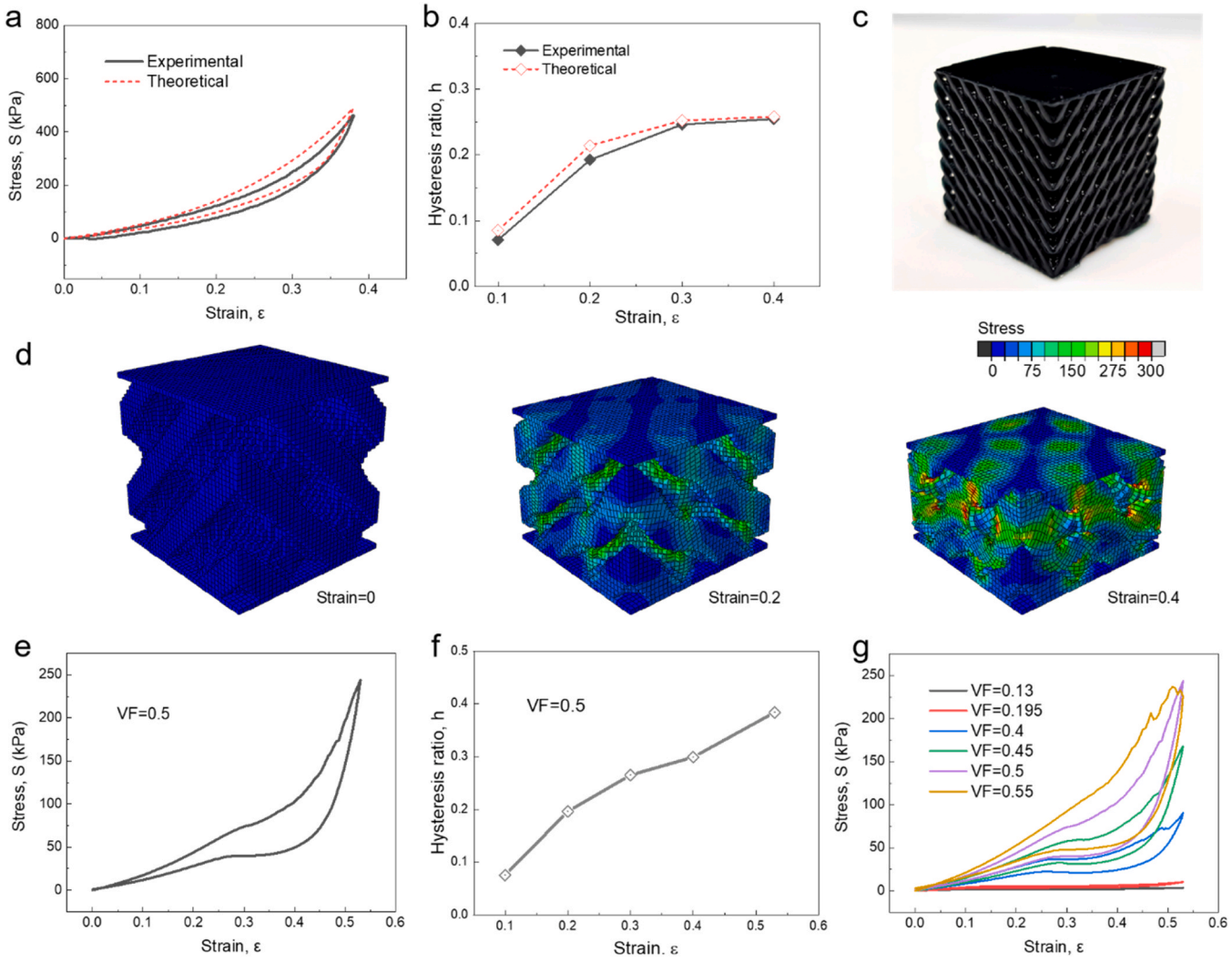


Fig. 5. Simulations on the mechanical behavior of bulk and structured hydrogels. (a) Comparison of experimental and theoretical stress-strain curves of bulk hydrogels; (b) Comparison of experimental and theoretical hysteresis ratios at various strains of bulk hydrogels; (c) 3D printing model of structured hydrogels; (d) The strain field in structured hydrogel under compressive loading test to various strains; (e) Theoretical stress-strain curve of a structured hydrogel with volume fraction of 0.5; (f) Theoretical hysteresis ratios of a structured hydrogel with volume fraction of 0.5 at various strains; (g) Theoretical stress-strain curves of structured hydrogels with different volume fractions.

presented in Fig. 5e and 5f. Consistent with the experimental trend, the structured model demonstrates a relatively flat stress-strain curve during small deformation and a notable stiffening during large deformation, leading to a lager hysteresis ratio. Furthermore, we explored the effect of the volume fraction of diamond structure on the mechanical behavior of the hydrogel. As illustrated in Fig. 5g, increasing the volume fraction resulted in a significant increase in stress, leading to a larger hysteresis ratio and a more pronounced strain stiffening. By utilizing the modified Ogden-Mullins model and conducting detailed investigations on structured hydrogels, the simulation enables visualization of the energy dissipation distribution within the hydrogel, which provides a better approach and framework for the design of anti-fatigue hydrogels for long-term energy harvesting.

Supplementary material related to this article can be found online at doi:10.1016/j.nanoen.2023.108857.

3.4. Demonstration towards practical application

Furthermore, in order to showcase the sensing potential of the developed 3D-ACH based samples, an extensive series of power generation characterizations were conducted, specifically utilizing practical finger-tapping actions. Fig. 6a illustrates the experimental setup, where finger-tapping motions were executed on the 3D-ACH sample, where the finger was enveloped with Al foil, applying various forces ranging from 0.02 to over 35 N (Fig. 6d and 6e). These forces were randomly applied during the experiments. The corresponding V_{OC} and I_{SC} outputs are shown in Fig. 6b and 6c, respectively. Upon thorough analysis of the acquired data, as shown in Fig. 6f and 6g, a notable linear relationship was observed between the applied force and both the current and voltage outputs, albeit with a logarithmic dependence. This discovery reinforces the significant potential of 3D-ACH for sensing applications. The concept of electrically stimulating tissues for regenerative purposes is an area of increasing interest within the scientific and medical communities. The application of electrical currents or fields to biological systems has shown potential in promoting cellular growth, guiding tissue development, and enhancing the regeneration process. However, despite these encouraging findings, the full extent of the benefits and underlying mechanisms are yet to be fully explored. Here, in order to simulate this scenario, Fig. 6h presents photographs of the coupling of a 3D-ACH sample with an artificial arthrosis. Benefits from its exceptional printing resolution and remarkable flexibility, the as-printed 3D-ACH sample exhibits excellent alignment and adhesion, even when faced with the intricate surface of artificial arthrosis. By altering the bending angles of the artificial arthrosis, different pressures are generated and applied mechanical input onto the printed sample (as shown in the supplementary video-2). Consequently, Fig. 6i and j exhibit a positive linear correlation between the bending angles of 5, 10, 15, and 20 degrees, and the corresponding V_{OC} and I_{SC} outputs (coefficient of determination, R^2 >0.99), which is consist with the V_{OC} result in Section 3.2. These findings highlight the ability of the 3D-ACH sample to effectively

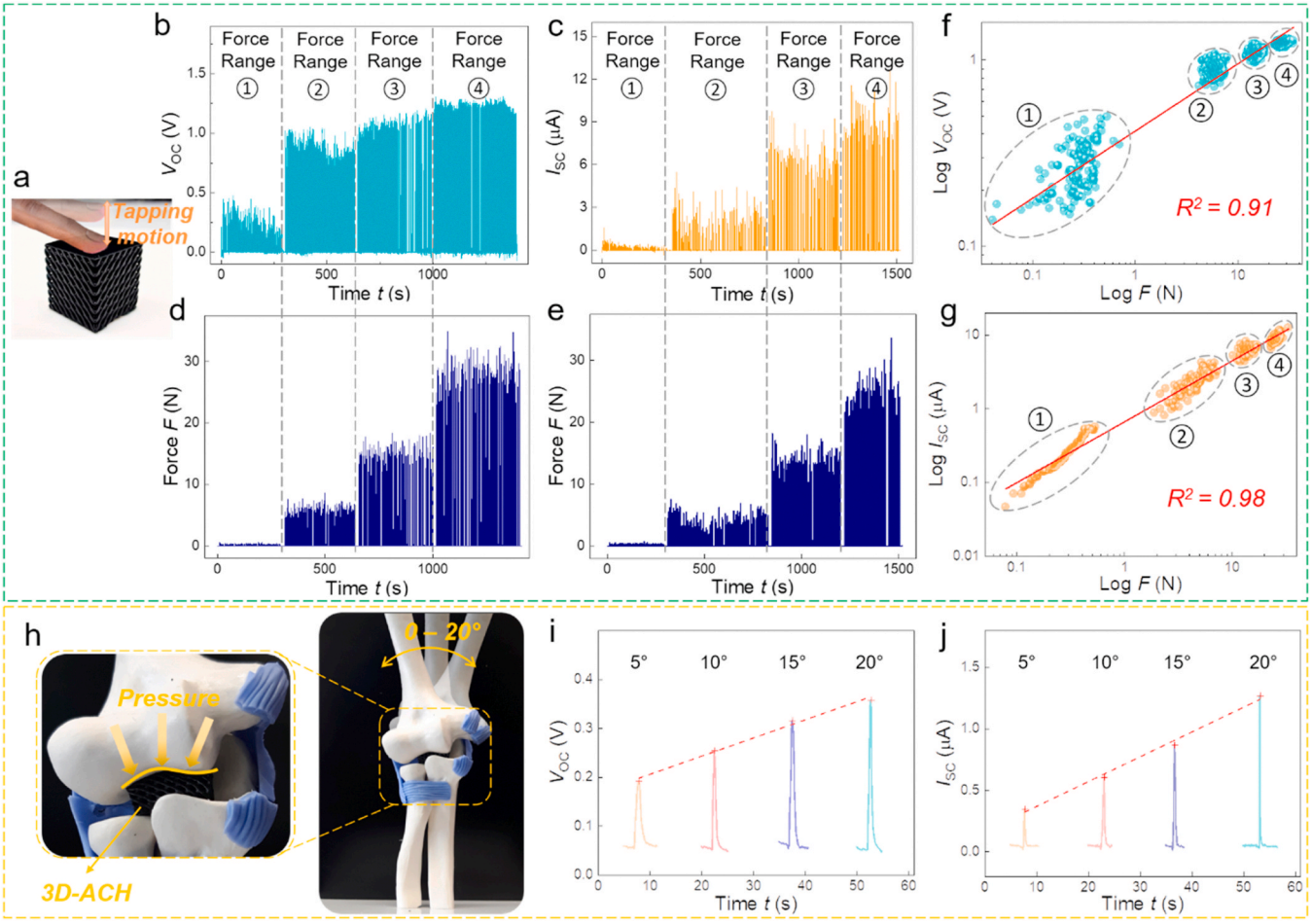


Fig. 6. (a) schematic illustration shows the hand tapping motion; The (b) V_{OC} and (c) I_{SC} outputs under random (d-e) hand tapping forces; Force-dependent logarithmic (f) V_{OC} and (g) I_{SC} outputs under random hand tapping; (h) Photographs showcasing the as-printed 3D-ACH coupled with an artificial arthrosis. By altering the bending angles of the artificial arthrosis, different pressures are generated; Consequently, the corresponding (i) V_{OC} and (j) I_{SC} outputs are shown for bending angles of 5, 10, 15, and 20 degrees. A strong linear correlation has been identified for both V_{OC} and I_{SC}, characterized by a fitting coefficient of determination, R^2> 0.99.

sense and respond to external forces, with the current and voltage outputs accurately reflecting the magnitude of the applied force. The linear relationship established between the force and the outputs further strengthens the viability of 3D-ACH for a wide range of sensing applications, confirming its promising future in the field.

Supplementary material related to this article can be found online at doi:10.1016/j.nanoen.2023.108857.

4. Conclusion

In summary, this study highlights the potential of integrating additive manufacturing with conductive hydrogels to create self-powered sensing devices. Through fast and high-resolution stereolithography printing, coupled with DC energy generation, the device enables self-powered sensing operations. The 3D-ACH exhibited impressive electrical performance, generating an open-circuit voltage of 1.15 V and a short-circuit current of up to 6.61 μA. These results indicate the device's potential for efficient energy generation. The energy generation mechanisms of the 3D-ACH encompass a multifaceted approach, incorporating tribovoltaic phenomena, ionic-electronic conduction, and electrochemistry. Furthermore, the printed architected conductive hydrogel exhibits an impressive combination of flexibility and mechanical strength, enabling it to withstand compressive strain of over 50% without sustaining any structural damage. These characteristics enable the device to function as a pressure/strain sensor, broadening its range of potential applications in self-powered sensing. The results demonstrate the potential for the development of robust, flexible, and biocompatible sensors that can operate autonomously, paving the way for innovative applications in the field of self-powered sensing.

CRediT authorship contribution statement

J.L., R.Y., and C.Z. conceived the idea of the work. R.Y. and Z.G. designed and conducted the experiments. Z.Y and S.L performed the analysis of mechanical properties of the materials. R.Y. and J.L. analyzed the results and wrote the manuscript. All authors contributed to the discussion and edition of the manuscript.

Declaration of Competing Interest

The authors declare that they have no known competing financial interests or personal relationships that could have appeared to influence the work reported in this paper.

Data Availability

Data will be made available on request.

Appendix A. Supporting information

Supplementary data associated with this article can be found in the online version at doi:10.1016/j.nanoen.2023.108857.

References

[1] Z. Zhao, K. Xia, Y. Hou, Q. Zhang, Z. Ye, J. Lu, Designing flexible, smart and self-sustainable supercapacitors for portable/wearable electronics: from conductive polymers, Chem. Soc. Rev. 50 (2021) 12702–12743, https://doi.org/10.1039/D1CS00800E.

[2] Y. Chang, L. Wang, R. Li, Z. Zhang, Q. Wang, J. Yang, C.F. Guo, T. Pan, First decade of interfacial iontronic sensing: from droplet sensors to artificial skins, Adv. Mater. 33 (2021), 2003464, https://doi.org/10.1002/adma.202003464.

[3] Y. Zhou, X. Xiao, G. Chen, X. Zhao, J. Chen, Self-powered sensing technologies for human Metaverse interfacing, Joule 6 (2022) 1381–1389, https://doi.org/10.1016/j.joule.2022.06.011.

[4] B. Shi, Z. Liu, Q. Zheng, J. Meng, H. Ouyang, Y. Zou, D. Jiang, X. Qu, M. Yu, L. Zhao, et al., Body-integrated self-powered system for wearable and implantable applications, ACS Nano 13 (2019) 6017–6024, https://doi.org/10.1021/acsnano.9b02233.

[5] Q. Zheng, Q. Tang, Z.L. Wang, Z. Li, Self-powered cardiovascular electronic devices and systems, Nat. Rev. Cardiol. 18 (2021) 7–21, https://doi.org/10.1038/s41569-020-0426-4.

[6] S. Huang, Y. Liu, Y. Zhao, Z. Ren, C.F. Guo, Flexible electronics: stretchable electrodes and their future, Adv. Funct. Mater. 29 (2019), 1805924, https://doi.org/10.1002/adfm.201805924.

[7] R. Yang, R. Xu, W. Dou, M. Benner, Q. Zhang, J. Liu, Semiconductor-based dynamic heterojunctions as an emerging strategy for high direct-current mechanical energy harvesting, Nano Energy 83 (2021), 105849, https://doi.org/10.1016/j.nanoen.2021.105849.

[8] H.-R. Lim, H.S. Kim, R. Qazi, Y.-T. Kwon, J.-W. Jeong, W.-H. Yeo, Advanced soft materials, sensor integrations, and applications of wearable flexible hybrid electronics in healthcare, energy, and environment, Adv. Mater. 32 (2020), 1901924, https://doi.org/10.1002/adma.201901924.

[9] D. Zhao, Y. Zhu, W. Cheng, W. Chen, Y. Wu, H. Yu, Cellulose-based flexible functional materials for emerging intelligent electronics, Adv. Mater. 33 (2021), 2000619, https://doi.org/10.1002/adma.202000619.

[10] K. Dong, X. Peng, Z.L. Wang, Fiber/Fabric-Based piezoelectric and triboelectric nanogenerators for flexible/stretchable and wearable electronics and artificial intelligence, Adv. Mater. 32 (2020), 1902549, https://doi.org/10.1002/adma.201902549.

[11] R. Yang, M. Benner, Z. Guo, C. Zhou, J. Liu, High-performance flexible schottky DC generator via metal/conducting polymer sliding contacts, Adv. Funct. Mater. 31 (2021), 2103132, https://doi.org/10.1002/adfm.202103132.

[12] P. Deng, Y. Wang, R. Yang, Z. He, Y. Tan, Z. Chen, J. Liu, T. Li, Self-powered smart textile based on dynamic schottky diode for human-machine interactions, Adv. Sci. 10 (2023), 2207298, https://doi.org/10.1002/advs.202207298.

[13] Y. Cheng, Y. Ma, L. Li, M. Zhu, Y. Yue, W. Liu, L. Wang, S. Jia, C. Li, T. Qi, et al., Bioinspired microspines for a high-performance spray Ti_3C_2Tx MXene-based piezoresistive sensor, ACS Nano 14 (2020) 2145–2155, https://doi.org/10.1021/acsnano.9b08952.

[14] Z. Ma, X. Xiang, L. Shao, Y. Zhang, J. Gu, Multifunctional wearable silver nanowire decorated leather nanocomposites for joule heating, electromagnetic interference shielding and piezoresistive sensing, Angew. Chem. 61 (2022), e202200705, https://doi.org/10.1002/anie.202200705.

[15] Q. Su, Q. Zou, Y. Li, Y. Chen, S.-Y. Teng, J.T. Kelleher, R. Nith, P. Cheng, N. Li, W. Liu, et al., A stretchable and strain-unperturbed pressure sensor for motion interference-free tactile monitoring on skins, Sci. Adv. 7 (2021), eabi4563, https://doi.org/10.1126/sciadv.abi4563.

[16] Y. Xiong, Y. Shen, L. Tian, Y. Hu, P. Zhu, R. Sun, C.-P. Wong, A flexible, ultra-highly sensitive and stable capacitive pressure sensor with convex microarrays for motion and health monitoring, Nano Energy 70 (2020), 104436, https://doi.org/10.1016/j.nanoen.2019.104436.

[17] F. Jiang, G. Thangavel, X. Zhou, G. Adit, H. Fu, J. Lv, L. Zhan, Y. Zhang, P.S. Lee, Ferroelectric modulation in flexible lead-free perovskite schottky direct-current nanogenerator for capsule-like magnetic suspension sensor, Adv. Mater. (2023), 2302815, https://doi.org/10.1002/adma.202302815.

[18] R. Yang, Z. He, S. Lin, W. Dou, Z.L. Wang, H. Wang, J. Liu, Tunable tribovoltaic effect via metal-insulator transition, Nano Lett. 22 (2022) 9084–9091, https://doi.org/10.1021/acs.nanolett.2c03481.

[19] J. Liu, A. Goswami, K. Jiang, F. Khan, S. Kim, R. McGee, Z. Li, Z. Hu, J. Lee, T. Thundat, Direct-current triboelectricity generation by a sliding Schottky nanocontact on MoS_2 multilayers, Nat. Nanotechnol. 13 (2018) 112–116, https://doi.org/10.1038/s41565-017-0019-5.

[20] K. Meng, X. Xiao, W. Wei, G. Chen, A. Nashalian, S. Shen, X. Xiao, J. Chen, Wearable pressure sensors for pulse wave monitoring, Adv. Mater. 34 (2022), 2109357, https://doi.org/10.1002/adma.202109357.

[21] J. Qin, L.-J. Yin, Y.-N. Hao, S.-L. Zhong, D.-L. Zhang, K. Bi, Y.-X. Zhang, Y. Zhao, Z.-M. Dang, Flexible and stretchable capacitive sensors with different microstructures, Adv. Mater. 33 (2021), 2008267, https://doi.org/10.1002/adma.202008267.

[22] T. Lv, R. Cheng, C. Wei, E. Su, T. Jiang, F. Sheng, X. Peng, K. Dong, Z.L. Wang, All-fabric direct-current triboelectric nanogenerators based on the tribovoltaic effect as power textiles, Adv. Energy Mater. (2023), 2301178, https://doi.org/10.1002/aenm.202301178.

[23] X. Han, G. Xiao, Y. Wang, X. Chen, G. Duan, Y. Wu, X. Gong, H. Wang, Design and fabrication of conductive polymer hydrogels and their applications in flexible supercapacitors, J. Mater. Chem. A 8 (2020) 23059–23095, https://doi.org/10.1039/D0TA07468C.

[24] A. Salehi, X. Fu, D.-H. Shin, F. So, Recent advances in OLED optical design, Adv. Funct. Mater. 29 (2019), 1808803, https://doi.org/10.1002/adfm.201808803.

[25] H. Shao, J. Fang, H. Wang, L. Dai, T. Lin, Polymer–metal Schottky contact with direct-current outputs, Adv. Mater. 28 (2016) 1461–1466, https://doi.org/10.1002/adma.201504778.

[26] Q. Zeng, Y. Lai, L. Jiang, F. Liu, X. Hao, L. Wang, M.A. Green, Integrated photorechargeable energy storage system: next-generation power source driving the future, Adv. Energy Mater. 10 (2020), 1903930, https://doi.org/10.1002/aenm.201903930.

[27] X. Liu, J. Liu, S. Lin, X. Zhao, Hydrogel machines, Mater. Today 36 (2020) 102–124, https://doi.org/10.1016/j.mattod.2019.12.026.

[28] X. Fan, W. Nie, H. Tsai, N. Wang, H. Huang, Y. Cheng, R. Wen, L. Ma, F. Yan, Y. Xia, PEDOT:PSS for flexible and stretchable electronics: modifications, strategies, and applications, Adv. Sci. 6 (2019), 1900813, https://doi.org/10.1002/advs.201900813.

[29] G. Li, C. Li, G. Li, D. Yu, Z. Song, H. Wang, X. Liu, H. Liu, W. Liu, Development of conductive hydrogels for fabricating flexible strain sensors, Small 18 (2022), 2101518, https://doi.org/10.1002/smll.202101518.

[30] Y.S. Zhang, A. Khademhosseini, Advances in engineering hydrogels, Science 356 (2017), eaaf3627, https://doi.org/10.1126/science.aaf3627.
[31] W. Kong, C. Wang, C. Jia, Y. Kuang, G. Pastel, C. Chen, G. Chen, S. He, H. Huang, J. Zhang, et al., Muscle-inspired highly anisotropic, strong, ion-conductive hydrogels, Adv. Mater. 30 (2018), 1801934, https://doi.org/10.1002/adma.201801934.
[32] L. Han, K. Liu, M. Wang, K. Wang, L. Fang, H. Chen, J. Zhou, X. Lu, Mussel-inspired adhesive and conductive hydrogel with long-lasting moisture and extreme temperature tolerance, Adv. Funct. Mater. 28 (2018), 1704195, https://doi.org/10.1002/adfm.201704195.
[33] T. Zhu, Y. Ni, G.M. Biesold, Y. Cheng, M. Ge, H. Li, J. Huang, Z. Lin, Y. Lai, Recent advances in conductive hydrogels: classifications, properties, and applications, Chem. Soc. Rev. 52 (2023) 473–509, https://doi.org/10.1039/D2CS00173J.
[34] Y. Zhou, C. Wan, Y. Yang, H. Yang, S. Wang, Z. Dai, K. Ji, H. Jiang, X. Chen, Y. Long, Highly stretchable, elastic, and ionic conductive hydrogel for artificial soft electronics, Adv. Funct. Mater. 29 (2019), 1806220, https://doi.org/10.1002/adfm.201806220.
[35] S. Qu, 3D printing of hydrogel electronics, Nat. Electron. 5 (2022) 838–839, https://doi.org/10.1038/s41928-022-00900-0.
[36] T. Zhou, H. Yuk, F. Hu, J. Wu, F. Tian, H. Roh, Z. Shen, G. Gu, J. Xu, B. Lu, et al., 3D printable high-performance conducting polymer hydrogel for all-hydrogel bioelectronic interfaces, Nat. Mater. 22 (2023) 895–902, https://doi.org/10.1038/s41563-023-01569-2.
[37] T. Distler, A.R. Boccaccini, 3D printing of electrically conductive hydrogels for tissue engineering and biosensors – a review, Acta Biomater. 101 (2020) 1–13, https://doi.org/10.1016/j.actbio.2019.08.044.
[38] H. Yuk, B. Lu, S. Lin, K. Qu, J. Xu, J. Luo, X. Zhao, 3D printing of conducting polymers, Nat. Commun. 11 (2020) 1604, https://doi.org/10.1038/s41467-020-15316-7.
[39] N. Anandakrishnan, H. Ye, Z. Guo, Z. Chen, K.I. Mentkowski, J.K. Lang, N. Rajabian, S.T. Andreadis, Z. Ma, J.A. Spernyak, et al., Fast stereolithography printing of large-scale biocompatible hydrogel models, Adv. Healthc. Mater. 10 (2021), 2002103, https://doi.org/10.1002/adhm.202002103.
[40] H. Wei, M. Lei, P. Zhang, J. Leng, Z. Zheng, Y. Yu, Orthogonal photochemistry-assisted printing of 3D tough and stretchable conductive hydrogels, Nat. Commun. 12 (2021) 2082, https://doi.org/10.1038/s41467-021-21869-y.
[41] C. Yang, Z. Suo, Hydrogel ionotronics, Nat. Rev. Mater. 3 (2018) 125–142, https://doi.org/10.1038/s41578-018-0018-7.
[42] I. Maskery, L.A. Parry, D. Padrão, R.J.M. Hague, I.A. Ashcroft, FLatt Pack: a research-focussed lattice design program, Addit. Manuf. 49 (2022), 102510, https://doi.org/10.1016/j.addma.2021.102510.
[43] Z.H. Guo, H.L. Wang, Y. Shao, L. Li, L. Jia, X. Pu, Flexible ionic diodes with high rectifying ratio and wide temperature tolerance, Adv. Funct. Mater. 32 (2022), 2112432, https://doi.org/10.1002/adfm.202112432.
[44] S. Lin, Z.Lin Wang, The tribovoltaic effect, Mater. Today 62 (2023) 111–128, https://doi.org/10.1016/j.mattod.2022.11.005.
[45] T. Zhang, S. Lin, H. Yuk, X. Zhao, Predicting fracture energies and crack-tip fields of soft tough materials, Extrem. Mech. Lett. 4 (2015) 1–8, https://doi.org/10.1016/j.eml.2015.07.007.
[46] J. Gwinner, Non-linear elastic deformations, Acta Appl. Math. 11 (1988) 191–193, https://doi.org/10.1007/BF00047287.
[47] R.W. Ogden, D.G. Roxburgh, A pseudo–elastic model for the Mullins effect in filled rubber, Proc. R. Soc. Lond. Ser. A 455 (1999) 2861–2877, https://doi.org/10.1098/rspa.1999.0431.



Ruizhe Yang is currently a Ph.D. candidate in Mechanical Engineering at the State University of New York at Buffalo supervised by Prof. Jun Liu. He received his M.S. in Mechanical Engineering from the State University of New York at Buffalo in 2018, and B.Eng. from Hebei University of Engineering in 2017. His research interest includes advanced energy materials and micro/nanoengineering technologies. He is a recipient of the Dean's Graduate Achievement Award (2023) and National Award for Outstanding Graduate Student Overseas (2022).



Dr. Zipeng Guo is an Assistant Professor of Industrial and Systems Engineering and an AMPrint Center faculty at the Rochester Institute of Technology. He received his Ph.D. degree (2023) from the State University of New York at Buffalo, where he was advised by Dr. Chi Zhou. Zipeng's current research focuses on multi-stage additive manufacturing processes for multi-scale and multi-functional 3D structures. He is a recipient of the Dean's Graduate Achievement Award in 2022, 3rd place in the NSF poster competition in 2022, and multiple NSF travel grants.



Dr. Zhaohan Yu is currently a Postdoctoral Research Associate in Mechanical Engineering at Michigan State University. She earned her Ph.D. degree (2022) and B.S. degree (2017) in Materials Processing Engineering from Huazhong University of Science and Technology. Her research focuses on the design, fabrication, and manufacturing of soft materials, with a specific emphasis on their applications in healthcare and sustainability.



Fengyin Du is currently a Ph.D candidate in Materials Science and Engineering at Southeast University, under the guidance of Prof. Changwen Miao. Presently, she is also a visiting Ph.D. student at Purdue University supervised by Prof. Tian Li. She received her M.S. and B.Eng. in Civil Engineering from Qingdao University of Technology, mentored by Prof. Zuquan Jin. She is a recipient of the National Scholarship for Graduate Students (2019). Her research primarily focuses on multi-functional building materials.



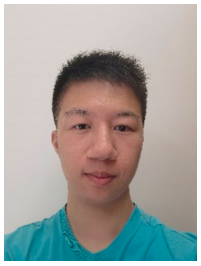
Vashin Gautham is currently a Ph.D. student in Mechanical Engineering supervised by Dr. Jun Liu. He received his M.S in Mechanical Engineering from University at Buffalo, SUNY in 2023 and B.E in Mechanical Engineering from RNSIT, VTU in 2020. He has worked on various projects during his academic journey from building a solar powered car, designing blades for helicopters to research in wearable, and self-powered sensing applications. His research interests include wearable devices, energy harvesting, self-powered devices using different energy materials and additive manufacturing



Leqi Lin received her M.S. in Mechanical Engineering at SUNY at Buffalo under Dr. Jun Liu's instruction in 2023. She holds another M.S. in Civil Engineering – Environmental engineering program (Advisor Dr.Wen Zhang) at New Jersey Institute of Technology in 2020, and B.S. in National Chung Cheng University, Taiwan in 2017. Her research interest includes flexible micro/nano engineering technologies and using Machine learning in sensor devices.



Dylan R. Yu is a high school student in the class of 2024 at Pittsford Mendon High School in upstate New York. He has maintained a position on the honor roll for his entire high school career thus far. He is working as a visiting student in Dr. Liu Jun's laboratory team. Currently, he is the president of Model United Nations at Pittsford Mendon High School as well as the secretary within his school's Science Olympiad team.



Pengchong Xu is currently an undergraduate student in Electrical Engineering, the Department of Electrical and Computer Engineering at Rutgers University. He is now working as a visiting student in Dr. Liu Jun's laboratory team. His research is focused on electromechanical coupling at material interfaces and developing novel sensors for pressure/friction sensing. He is also dedicated to exploring new applications with the novel sensor devices



Dr. Jason N. Armstrong is currently an Associate Professor of Teaching in the Department of Mechanical and Aerospace Engineering at the University at Buffalo. He is also the Director of Undergraduate Studies for Mechanical Engineering and runs the MAE Materials Teaching Laboratories. Research interests include mechanical properties & characterization, electrical & thermal performance, and sustainability. He has nearly 20 years of experience with materials characterization and design of experimental equipment.



Dr. Shaoting Lin holds the position of Assistant Professor in Mechanical Engineering at Michigan State University. He earned his Ph.D. degree (2019) at MIT and got his M.S. degree (2013) and B.S. degree (2010) at Tsinghua University. Dr. Lin has been focused on fundamental problems associated with the mechanical failures of soft materials and the longevity of soft machines. Dr. Lin was the co-founder of the EASF_Young Webinar (2020), the Executive Editorial Board Member of Giant (2022), and the Editor of the ASME Technical Committee of Mechanics of Soft Materials (2023).



Dr. Chi Zhou is an Associate Professor in the Department of Industrial and Systems Engineering at the University at Buffalo. He received his Ph.D. degree in Industrial and Systems Engineering from the University of Southern California (USC) in 2012 and his master's degree in Computer Science from USC in 2010. Prior to joining UB in July 2013, Zhou was a senior research and development engineer at EnvisionTec Inc. Dr. Zhou's current research focuses on additive manufacturing (3D printing) process modeling and optimization for advanced materials including nano- and bio- materials.



Dr. Jun Liu is currently an 1 Assistant Professor in the Department of Mechanical and Aerospace Engineering at The State University of New York at Buffalo, USA. He is also an affiliated faculty in RENEW Institute at UB. Prior to join UB, He received his Ph.D. in Materials Engineering from the University of Alberta, Canada in 2018. He is also an Associate Editor of Energy Technology (Wiley). He is the recipient of many distinguished awards and honors such as SONY 2021 Faculty Innovation Award and Microsystem and Nanoengineering (MINE) 2020 Young Scientist Award (Nature Springer).